10.1071/WF23050
International Journal of Wildland Fire

Supplementary Material

A laboratory-scale simulation framework for analysing wildfire hydrologic and water quality effects

Carli P. Brucker[A,B,C,*], *Ben Livneh*[A,B], *Claire E. Butler*[D] and *Fernando L. Rosario-Ortiz*[A,E]

[A]Department of Civil, Environmental, and Architectural Engineering, University of Colorado Boulder, Discovery Drive, Boulder, CO 80309, USA

[B]Cooperative Institute for Research in Environmental Sciences, University of Colorado Boulder, Discovery Drive, Boulder, CO 80309, USA

[C]Carollo Engineers, 11030 Circle Point Road, Suite 400, Westminster, CO 80020, USA

[D]Department of Chemical and Environmental Engineering, Yale University, New Haven, CT 06520, USA

[E]Environmental Engineering Program, University of Colorado Boulder, Boulder, CO 80309, USA

*Correspondence to: Email: carli.brucker@colorado.edu

Supplement A: Experimental Method and Simulator Component Design

Wildfire Simulator Burn Intensity Characterization

Six methods of burn intensity characterization were initially evaluated for use in this study. Fig. S1 shows boxplots of suspended sediment concentration, as an example, binned into increasing burn intensity increments using each characterization method. 'Peak temperature' and 'Peak temperature (data logger)' were measurements of peak soil sample surface temperatures achieved, derived from visual inspections of the data loggers during burning and a post-burn assessment of time-temperature curves, respectively. These temperatures were then binned into a temperature-based burn intensity scale derived from previous literature (discussed further below). 'Degree hours' were characterizations based on both temperature and time, calculated by integrating under samples' entire time-temperature curves. 'Modified degree hours' were similarly based on temperature and time, though this metric was calculated by integrating under time temperature curves just until peak surface temperatures were achieved. Both of these metrics were binned into discrete burn intensity characterizations with cutoffs based on their terciles. The 'Luminance' characterization metric, or measure of light reflectance per unit area (Toivanen *et al.* 2000), was based on the reflectance of samples derived from image processing, with intensity bins similarly based on the metric's terciles. Finally, 'Visual' characterizations of burn intensity were completed by two separate researchers, using U.S. Forest Service burn severity methods as a guide (Parson *et al.* 2010). Analysis of variance (ANOVA) tests for each characterization method show whether all burn intensity groups are significantly difference from

all other groups (α = 0.05).

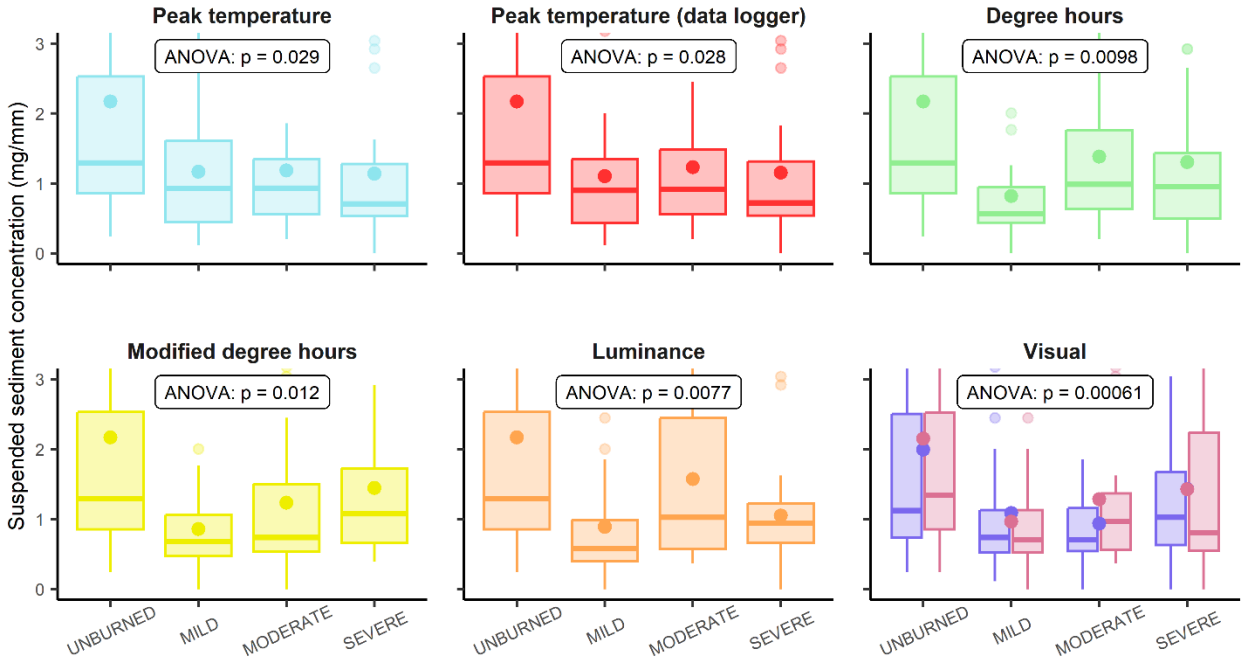

Fig. S1. Boxplots of suspended sediment concentration, as an example, with increasing burn intensity increments characterized using each of the six methods evaluated in this study.

Temperature-based and "degree-hours" scales—a metric which incorporates both temperature and duration (Blank *et al.* 1994; Lentile *et al.* 2006; Keeley 2009; Stoof *et al.* 2011; Cancelo-González *et al.* 2012; Wang *et al.* 2015)—were the burn intensity characterization methods ultimately chosen due to their allowance for quantification and repeatable intensity treatments. The temperature-based scale was used for completing initial replicates in the experimental matrix, with samples secondarily characterized by degree hour intensities during post-experimental analyses.

The temperature-based characterization was based on peak temperatures achieved at the 'hottest' lateral location on each soil sample's surface during burn simulations. This was measured by thermocouples placed at multiple lateral positions across samples' surfaces, as

described in the *Wildfire Simulator Design and Procedure* section in the manuscript. As of yet, no universal surface temperature-based wildfire intensity scale exists (Keeley 2009; Moody *et al.* 2013), as qualitative characterizations of burn severity such as the type of vegetation consumed (Emmerich and Cox 1992; Nyman *et al.* 2014) or ash color (Moreno and Oechel 1989) are more typical in wildfire studies (Keeley 2009; Brucker *et al.* 2022). Thus, we created a unique scale based on temperature-severity characterizations referenced across previous studies (Chandler *et al.* 1983; Robichaud and Hungerford 2000; Wang *et al.* 2015; Wieting *et al.* 2017; Jian *et al.* 2018; Hohner *et al.* 2019), as seen in Table 2 in the manuscript.

Degree-hours were calculated for each sample by interpolating under time-temperature curves associated with the 'hottest' area of samples' surfaces, i.e., using the same thermocouple measurements as the temperature-based characterization. As seen in Fig. 6a in the manuscript, the area under the time-temperature curve was summed at 5 s intervals from the beginning of the simulation until temperatures had cooled to less than ~100°C, with initial ambient temperature subtracted. The equation used to calculate this metric was a slightly altered version of the equation from Cancelo-González et al., 2012:

$$DH = \sum (T_S - T_{Amb.}) * (5\ \text{sec}) * (\frac{1\ hr}{3600\ \text{sec}})$$

(**Eqn. S1**)

Where DH = degree-hour in °C-h, T_S = the surface temperature at each 5 s interval in °C, and $T_{Amb.}$ = the ambient temperature recorded at the start of the wildfire simulation in °C. As no standardized intensity categorization of degree-hours exists, burned samples were characterized as 'mild', 'moderate', or 'severe' using terciles of all degree-hour values calculated from the experiment. Note, as burn intensities were characterized using the thermocouple location with

the highest achieved surface temperatures for both methods, soil samples in aggregate likely achieved lower, more spatially variable burn intensities.

While temperature-based and degree hour characterizations were similar for each burned soil sample, important differences resulted in distinct relationships with hydrologic and water quality responses. Degree hours generally trended linearly with surface temperatures as shown in Fig. S2, with an $R^2 = 0.77$ correlation when degree hour outliers (values greater than one standard deviation above the median) were removed. However, degree hours values varied greatly for samples heated to temperatures above ~500°C, due to high variability of heating ramp-up and cool-down times during severe burn simulations. Due to these differences, results showed that peak temperature (highlighted by the temperature-based characterization) may have been a stronger driving mechanism for runoff and solute responses, whereas heating durations (highlighted by degree hours) affected sedimentation and turbidity responses more strongly. When compared to the temperature-based scale, runoff ratios at 30° terrain slopes showed significant (ANOVA test *p*-value of 0.036) monotonic increases from low to high burn intensities, while trends were non-existent when compared to degree hours. DOC and TDN showed significant inverse 'U' shaped trends with increasing temperature-based burn intensities, but similarly lacked trends when compared to degree hours. Suspended sediment concentration (SSC) and turbidity were more strongly correlated with degree hours than surface temperatures, however, showing significant (ANOVA *p*-values of 0.013 and 0.033, respectively monotonic increases with increasing degree hours (at a 20° terrain slope for turbidity).

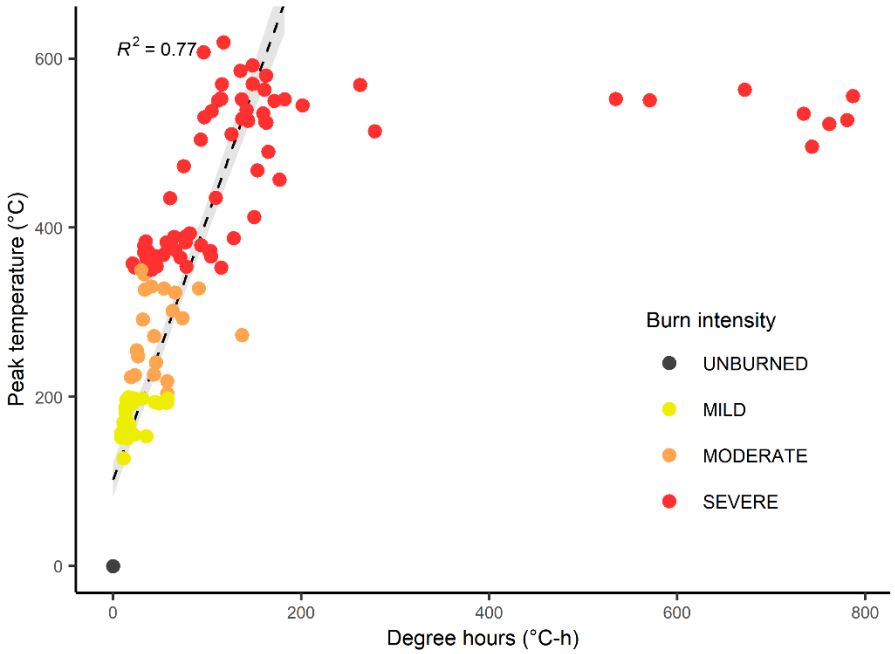

Fig. S2. The relationship between peak soil surface temperatures measured during burn simulations and calculated degree hours. A linear relationship for lower intensity burn values is shown by a dashed line—the best linear fit ($R^2 = 0.77$) with degree hour outliers (values greater than one standard deviation above the median) removed. The shaded area represents the confidence intervals (level = 0.95). Different colors represent samples' burn intensities characterized using the temperature-based scale.

Soil Sampling Container, Tilting Mechanism, and Custom Funnel Design

After excavation, soil samples were placed in unique sampling containers to minimize structural degradation during transportation and edge effects during testing. Sampling containers were designed to withstand intense heat from wildfire simulations and allow for collection of sample runoff and percolation. Containers were created from rectangular 30.5 x 10.2 cm steel pipes with 1.3 cm thick walls, which were cut to 10.2 cm segments. Selected for their high melting point, these steel piping-based sampling containers were similar to those in Stoof et al., 2011, also with

holes for thermocouple insertion drilled into the sides. Use of piping allowed for both applied precipitation and sample percolation collection, though the rectangular shape was more conducive to capturing runoff (Cancelo-González *et al.* 2013; Keesstra *et al.* 2014; Kibet *et al.* 2014) compared with circular piping used in other sampling containers (Busse *et al.* 2010; Wieting *et al.* 2017).

These sampling containers fit into custom funnels designed to capture hydrologic responses, which also interfaced with the tilting mechanism described in the manuscript. For the tilting mechanism, a 0.7 x 1.0 m aluminum frame was constructed to pivot at the back of the rainfall simulator while resting on an adjustable rod at the front, placed at different vertical locations to set terrain slopes. Graduated cylinders at all four sides of the tilting mechanism measured simulated precipitation, affixed using bracket sets which positioned them at constant lateral locations for all three terrain slopes. Following a similar design concept as Kibet et al., 2014, aluminum funnels were designed and created to hold soil samples in the tilting mechanism, separating and collecting runoff and percolation generated by precipitation. Bracket sets for the funnels were placed on the tilting frame to hold their lateral positions constant, similar to the graduated cylinders. The runoff collection chamber was placed at the ‘downhill’ end of the funnel, covered by an angled piece of aluminum to deflect precipitation, with the percolation chamber underneath the sample. Small plastic funnels were affixed to the bottom of each chamber, channeling liquids through attached plastic tubes which led to sample bottles placed outside the simulator.

Water Quality Analysis Methods

Runoff samples were defrosted, then analyzed in a lab to assess total suspended solids (TSS), dissolved organic carbon (DOC), and total dissolved nitrogen (TDN) levels, as well as turbidity.

Turbidity was first measured by gently inverting each sample several times to homogenize suspended solids, then testing a 30 mL subset in a Hach 2100N Turbidimeter. To measure TSS, samples were first filtered using a vacuum pump through 0.7 µm glass filters, which were then dried in an ~104°C oven for 1 h. These were weighed before and after filtering to determine collected sediment mass. The filtered liquid was then tested for DOC and TDN using a Shimadzu TOC-V/TN Analyzer. Samples were prepared by pouring them into 24 mL glass vials and adding 1M of hydrochloric acid, acidifying them to a pH of 2-3 (Shimadzu Corporation 2001). The Shimadzu instrument then measured DOC by sparging samples with high-purity air, removing inorganic carbon (i.e. carbonates and bicarbonates), then determining the non-purgeable organic carbon (Shimadzu Corporation 2001). TDN was measured simultaneously through a similar oxidation process. The machine's calibration curves were created using a standard, with peak DOC and TDN concentrations of 25 and 5 mg/L, respectively. Samples with higher concentrations were re-tested with a 1:1 dilution.

Though the USEPA method 415.3 defines dissolved constituents as < 0.45 µm (Potter and Wimsatt 2012), the 0.7 µm filters used for TSS analysis were also deemed sufficient for DOC and TDN testing. Samples filtered through this size had similar solute concentrations to those filtered at 0.45 µm and fulfilled requirements for testing on the Shimadzu TOC-V/TN Analyzer (Shimadzu Corporation 2001). Pairwise t-tests performed on six samples filtered separately through 0.7 µm and 0.45 µm filters showed no significant differences in dissolved organic carbon (DOC) and total dissolved nitrogen (TDN) concentrations ($p = 0.74$ and $p = 0.50$, respectively), with median absolute differences of 5.8% and 4.0% (ranges of -7.2 to 10.9% and -5.7 to 15.3% differences), respectively, between the two sizes. Comparatively, median absolute differences in duplicates (samples tested multiple times during the same run) across all samples

were slightly lower, or 1.4% and 1.8% for DOC and TDN concentrations, respectively, but with wider ranges of percent differences, or -48.8 to 14.2% and -63.6 to 15.6%, respectively. Thus, the differences in concentrations produced by the two filter sizes was deemed marginal—no higher than the existing variability between duplicate samples generated by experimental error. Additionally, 0.7 µm filter sizes were within specifications for testing on the Shimadzu TOC-V/TN Analyzer, which required use of 1.5 µm filter sizes or finer (Shimadzu Corporation 2001).

Supplement B: Results from Samples Tested in Experimental Matrix

Sequential Rainfall Treatments

Outside of samples tested in the experimental matrix, 27 additional samples from varying burn intensities were subjected to two sequential rainfall treatments. These samples either received first low intensity (~14.4 mm/h) precipitation for 2 h, then high intensity (~51.3 mm/h) for 2 h, or vice versa, with a ~24 h drying period in between. Fig. S3 shows medians of runoff ratios at each timestep in the rainfall simulations for the first and second rainfall treatments. The second precipitation events typically generated more runoff than first events with equivalent rainfall intensities, with median runoff ratios for the second treatments almost 50% higher than the first treatments. This relationship was slightly heightened with increasing burn intensity, with median runoff ratios for second treatments ~73% higher than first treatments for severely burned samples. As seen in Fig. S4, water quality responses were slightly lower for the second treatments than the first, with median values ~20, 5, 42, and 28% lower than the first treatments for SSC, DOC, TN, and turbidity, respectively.

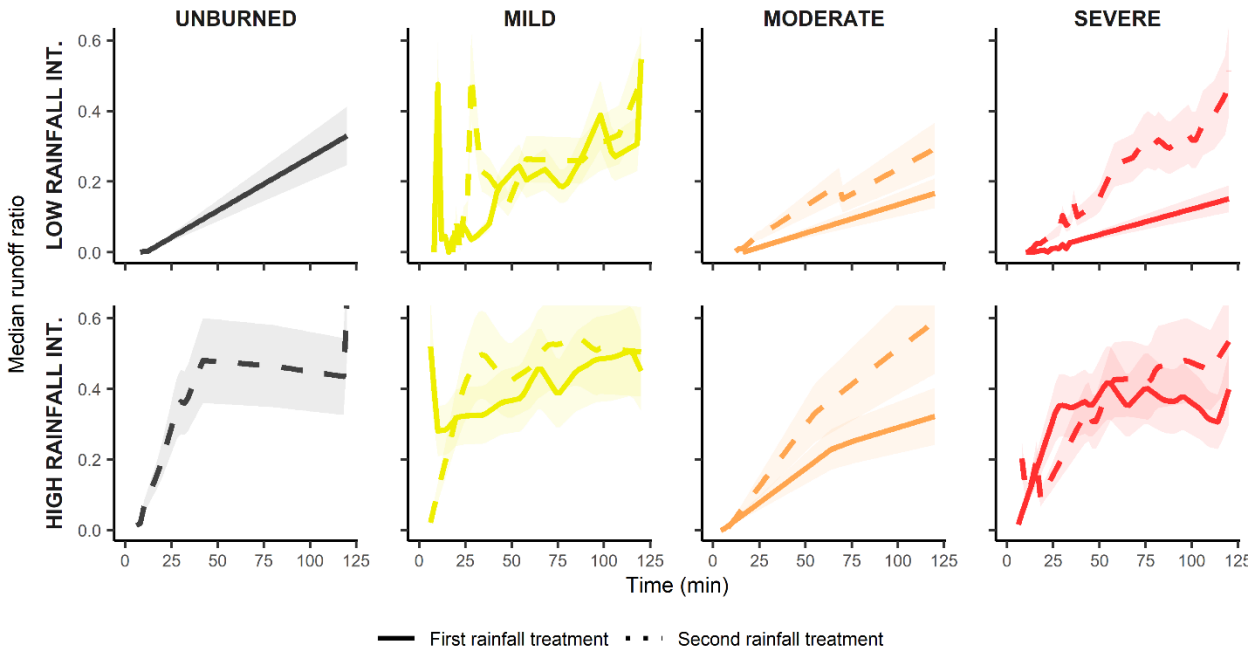

Fig. S3. Time series plots of median runoff ratios from soil samples which received two sequential rainfall treatments, with a ~24 h drying period in between. Responses for low (~14.4 mm/h) and high (~51.3 mm/h) rainfall intensities are shown in the top and bottom rows, respectively. Colors represent different burn intensities, with the solid lines showing responses from the first rainfall treatments and the dashed lines representing the second treatments. Shaded areas represent the interquartile ranges.

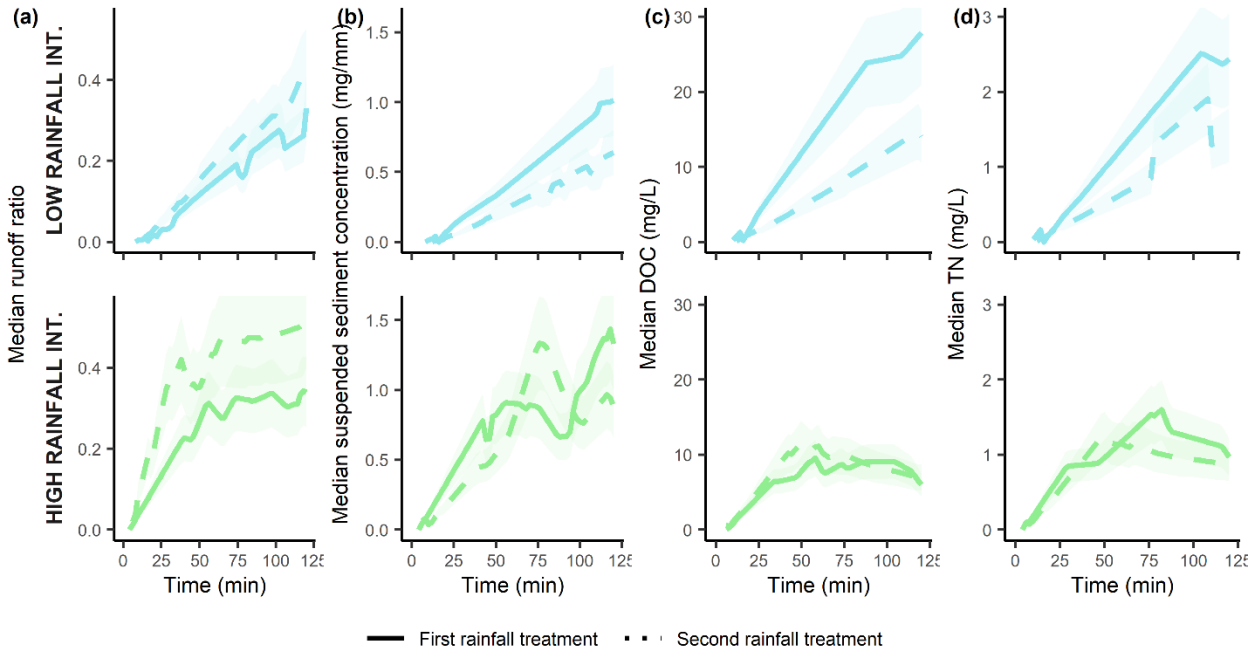

Fig. S4. Time series plots of median runoff ratio, suspended sediment concentration, DOC, and TDN responses from samples subjected to two sequential rainfall events, with a ~24 h drying period in between. Responses for low (~14.4 mm/h) and high (~51.3 mm/h) rainfall intensities are shown in the top and bottom rows, respectively. Colors represent these two treatment options, with the solid lines showing responses from the first rainfall treatments and the dashed lines representing the second treatments. Shaded areas represent the interquartile ranges.

Supplement C: Experimental Limitations

Mass Loss During Burn Simulation

As discussed in the *Experimental Limitations* section of the manuscript, extra handling of burned samples may have contributed to higher sediment response in unburned samples. As seen in Fig. S5, high mass loss occurred during this step up to ~15% of samples' weights.

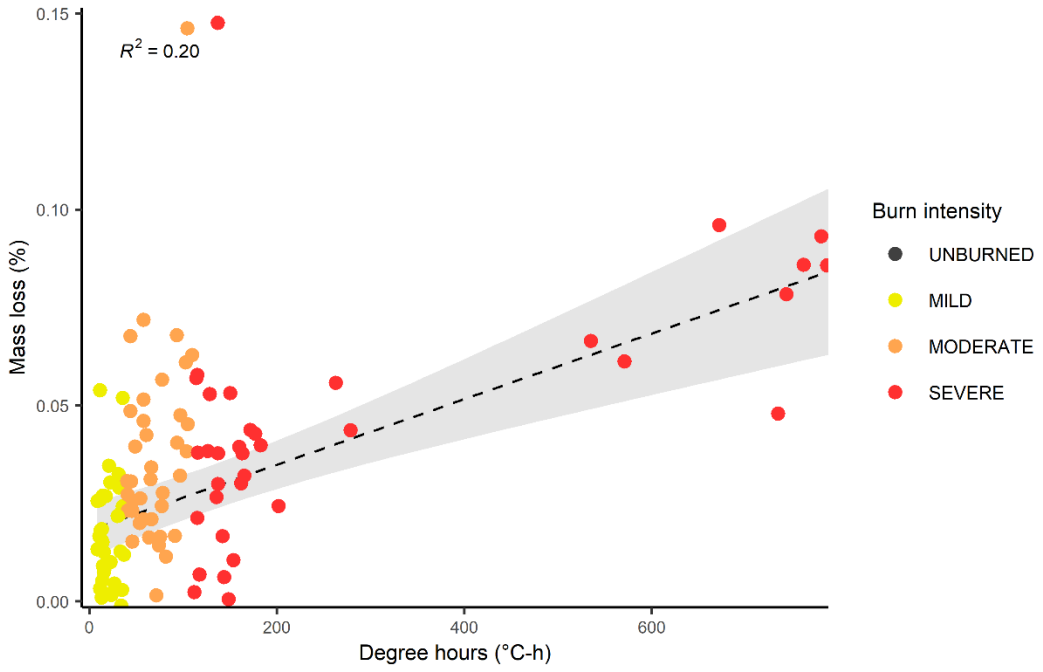

Fig. S5. Soil sample mass loss, or the percent change in weight after burning, plotted against degree hours achieved. Point colors represent different burn intensities. The dashed line represents the best linear fit of the data, with an $R^2 = 0.20$, and the shaded area shows the confidence interval (level = 0.95).

Water and Sediment Loss During Rainfall Simulation

Comparisons of storage estimates and changes in soil moisture for each sample revealed system losses during rainfall simulation. Storage was estimated by closing samples' water balance equations, as discussed in the *Experimental Limitations* section in the manuscript, made under the assumption that no losses occurred during simulation. However, this was unlikely due to abstractions and unaccounted flow paths throughout the system. Thus, these estimates were compared to the change in volumetric soil moisture in several soil samples before and after simulation, with values converted to depths by using the samples' weights and common physical characteristics for loamy sand.

As shown in Fig. S6a, little to no trend was apparent in storage estimates with increasing burn intensity, whereas change in soil moisture generally increased monotonically with increasing intensities—indicating potential inaccuracies in the estimates. Storage values were somewhat linearly related to change in soil moisture, as shown in Fig. S6b, with R^2 values up to 0.47 for specific burn intensities when values were expressed as percentages of total precipitation. However, these estimates were generally greater than soil moisture changes, or up to a difference of 91% of precipitation. Storage estimates were closest to changes in soil moisture for unburned samples, with a median difference of storage from moisture change of 2.9% of precipitation. Mild, moderate, and severe intensities had median differences of 43, 43, and 28%, respectively. These larger differences in burned samples as compared with unburned samples indicate greater liquid and sediment loss during rainfall simulations for these samples—further explaining previously discussed anomalous responses.

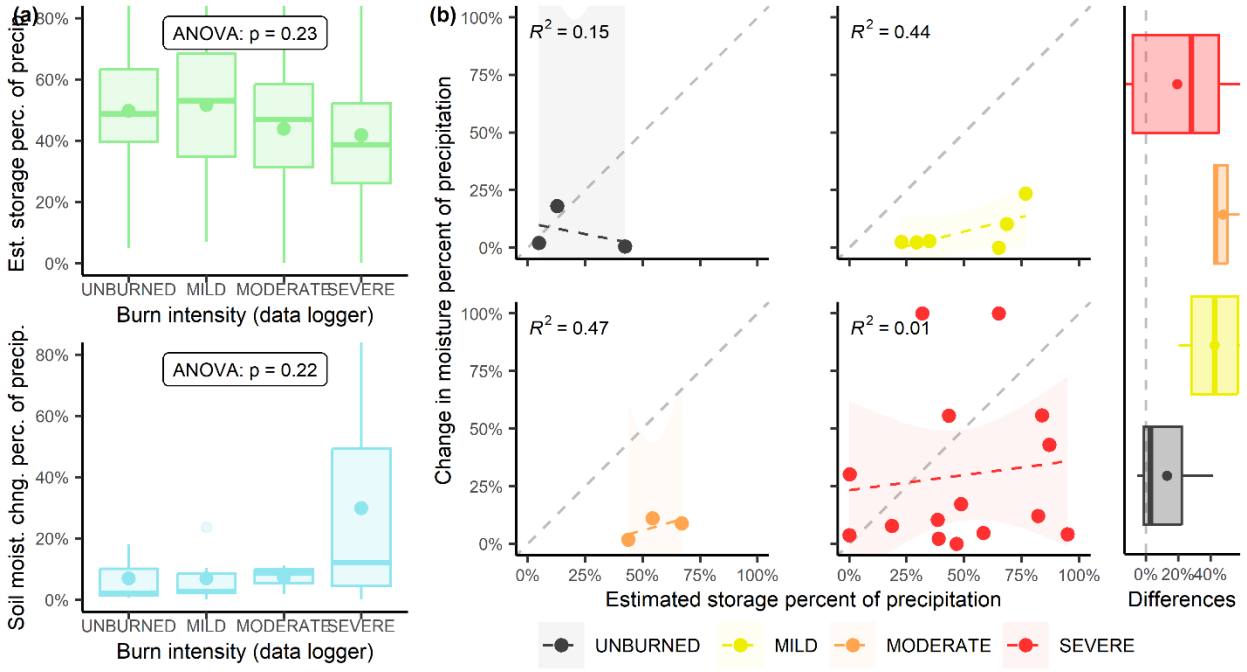

Fig. S6. (a) Boxplots of estimated storage and soil moisture change values expressed as percentages of total precipitation for 27 individual soil samples, plotted with increasing burn intensity. (b) Change in soil moisture during rainfall simulation for each sample plotted against estimated storage during the event, expressed as percentages of total precipitation. Plots are divided into unburned, mild, moderate, and severe burn intensities, with best linear fits represented by dashed lines and R^2 values of 0.15, 0.44, 0.47, and 0.01, respectively. Shaded areas represent confidence intervals (level = 0.95), with a gray, dashed 1:1 line in the background. A boxplot displays differences in storage from change in soil moisture for each burn intensity, expressed as percentages of total precipitation. Colors represent different burn intensities.

References

Blank RR, Allen F, Young JA (1994) Extractable Anions in Soils following Wildfire in a Sagebrush-Grass Community. *Soil Science Society of America Journal* **58**, 564–570. doi:10.2136/sssaj1994.03615995005800020045x.

Brucker CP, Livneh B, Minear JT, Rosario F (2022) A review of simulation experiment techniques used to analyze wildfire effects on water quality and supply. *Environmental Science: Processes & Impacts*.

Busse MD, Shestak CJ, Hubbert KR, Knapp EE (2010) Soil Physical Properties Regulate Lethal Heating during Burning of Woody Residues. *Soil Science Society of America Journal* **74**, 947–955. doi:10.2136/sssaj2009.0322.

Cancelo-González J, Barros N, Rial-Rivas ME, Díaz-Fierros F (2012) Assessment of the impact of soil heating on soil cations using the degree-hours method . *Spanish Journal of Soil Science* **2**,. doi:10.3232/SJSS.2012.V2.N3.04.

Cancelo-González J, Rial-Rivas ME, Díaz-Fierros F (2013) Effects of fire on cation content in water: a laboratory simulation study. *International Journal of Wildland Fire* **22**, 667–680. doi:10.1071/WF12178.

Chandler C, Cheney P, Thomas P, Trabaud L, Williams D (1983) 'Fire in forestry. Volume 1. Forest fire behavior and effects. Volume 2. Forest fire management and organization.' (John Wiley & Sons, Inc.: New York)

Emmerich WE, Cox JR (1992) Hydrologic characteristics immediately after seasonal burning on introduced and native grasslands. *Rangeland Ecology & Management / Journal of Range Management Archives* **45**, 476–479.

Hohner AK, Summers RS, Rosario-Ortiz FL (2019) Laboratory simulation of postfire effects on conventional drinking water treatment and disinfection byproduct formation. *AWWA Water Science* **1**, e1155. doi:10.1002/aws2.1155.

Jian M, Berli M, Ghezzehei TA (2018) Soil Structural Degradation During Low-Severity Burns. *Geophysical Research Letters* **45**, 5553–5561. doi:10.1029/2018GL078053.

Keeley JE (2009) Fire intensity, fire severity and burn severity: a brief review and suggested usage. *International Journal of Wildland Fire* **18**, 116–126. doi:10.1071/WF07049.

Keesstra SD, Maroulis J, Argaman E, Voogt A, Wittenberg L (2014) Effects of controlled fire on hydrology and erosion under simulated rainfall. *Cuadernos de Investigación Geográfica* **40**, 269–294. doi:10.18172/cig.2532.

Kibet LC, Saporito LS, Allen AL, May EB, Kleinman PJA, Hashem FM, Bryant RB (2014) A Protocol for Conducting Rainfall Simulation to Study Soil Runoff. *Journal of Visualized Experiments : JoVE*. doi:10.3791/51664.

Lentile LB, Holden* ZA, Smith* AMS, Falkowski MJ, Hudak AT, Morgan P, Lewis SA, Gessler PE, Benson NC (2006) Remote sensing techniques to assess active fire characteristics and post-fire effects. *International Journal of Wildland Fire* **15**, 319–345. doi:10.1071/WF05097.

Moody JA, Shakesby RA, Robichaud PR, Cannon SH, Martin DA (2013) Current research issues related to post-wildfire runoff and erosion processes. *Earth-Science Reviews* **122**, 10–37. doi:10.1016/j.earscirev.2013.03.004.

Moreno JM, Oechel WC (1989) A simple method for estimating flre intensity after a burn in California chaparral. *Acta Oecol* 13.

Nyman P, Sheridan GJ, Smith HG, Lane PNJ (2014) Modeling the effects of surface storage, macropore flow and water repellency on infiltration after wildfire. *Journal of Hydrology* **513**, 301–313. doi:10.1016/j.jhydrol.2014.02.044.

Parson A, Robichaud PR, Lewis SA, Napper C, Clark JT (2010) Field guide for mapping post-fire soil burn severity. *Gen Tech Rep RMRS-GTR-243 Fort Collins, CO: US Department of Agriculture, Forest Service, Rocky Mountain Research Station 49 p* **243**,. doi:10.2737/RMRS-GTR-243.

Potter BB, Wimsatt JC (2012) USEPA method 415.3: Quantifying TOC, DOC, and SUVA. *Journal-American Water Works Association* **104**, E358–E369.

Robichaud PR, Hungerford RD (2000) Water repellency by laboratory burning of four northern Rocky Mountain forest soils. *Journal of Hydrology* **231–232**, 207–219. doi:10.1016/S0022-1694(00)00195-5.

Shimadzu Corporation (2001) TOC-Vcsh/csn Total Organic Carbon User Manual.

Stoof CR, De Kort A, Bishop TFA, Moore D, Wesseling JG, Ritsema CJ (2011) How Rock Fragments and Moisture Affect Soil Temperatures during Fire. *Soil Science Society of America Journal* **75**, 1133–1143. doi:10.2136/sssaj2010.0322.

Toivanen P, Hovila J, Kärhä P, Ikonen E (2000) Realizations of the units of luminance and spectral radiance at the HUT. *Metrologia* **37**, 527. doi:10.1088/0026-1394/37/5/40.

Wang J-J, Dahlgren RA, Erşan MS, Karanfil T, Chow AT (2015) Wildfire Altering Terrestrial Precursors of Disinfection Byproducts in Forest Detritus. *Environmental Science & Technology* **49**, 5921–5929. doi:10.1021/es505836m.

Wieting C, Ebel BA, Singha K (2017) Quantifying the effects of wildfire on changes in soil properties by surface burning of soils from the Boulder Creek Critical Zone Observatory. *Journal of Hydrology: Regional Studies* **13**, 43–57. doi:10.1016/j.ejrh.2017.07.006.